NeuroImage xx (xxxx) xxxx–xxxx

Contents lists available at ScienceDirect

NeuroImage

journal homepage: www.elsevier.com/locate/neuroimage

Exploring sex differences in the adult zebra finch brain: *In vivo* diffusion tensor imaging and *ex vivo* super-resolution track density imaging

Julie Hamaide[a], Geert De Groof[a], Gwendolyn Van Steenkiste[b], Ben Jeurissen[b], Johan Van Audekerke[a], Maarten Naeyaert[a], Lisbeth Van Ruijssevelt[a], Charlotte Cornil[c], Jan Sijbers[b], Marleen Verhoye[a], Annemie Van der Linden[a,*]

[a] *Bio-Imaging Lab, Department of Biomedical Sciences, University of Antwerp, Belgium*
[b] *iMinds-Vision Lab, Department of Physics, University of Antwerp, Belgium*
[c] *GIGA Neurosciences, Research Group in Behavioral Neuroendocrinology, University of Liège, Belgium*

ARTICLE INFO

Keywords:
DTI
Zebra finch
Super-resolution reconstruction
Voxel-based analysis
Tractography
Songbird

ABSTRACT

Zebra finches are an excellent model to study the process of vocal learning, a complex socially-learned tool of communication that forms the basis of spoken human language. So far, structural investigation of the zebra finch brain has been performed *ex vivo* using invasive methods such as histology. These methods are highly specific, however, they strongly interfere with performing whole-brain analyses and exclude longitudinal studies aimed at establishing causal correlations between neuroplastic events and specific behavioral performances. Therefore, the aim of the current study was to implement an *in vivo* Diffusion Tensor Imaging (DTI) protocol sensitive enough to detect structural sex differences in the adult zebra finch brain. Voxel-wise comparison of male and female DTI parameter maps shows clear differences in several components of the song control system (*i.e.* Area X surroundings, the high vocal center (HVC) and the lateral magnocellular nucleus of the anterior nidopallium (LMAN)), which corroborate previous findings and are in line with the clear behavioral difference as only males sing. Furthermore, to obtain additional insights into the 3-dimensional organization of the zebra finch brain and clarify findings obtained by the *in vivo* study, *ex vivo* DTI data of the male and female brain were acquired as well, using a recently established super-resolution reconstruction (SRR) imaging strategy. Interestingly, the SRR-DTI approach led to a marked reduction in acquisition time without interfering with the (spatial and angular) resolution and SNR which enabled to acquire a data set characterized by a 78 μm isotropic resolution including 90 diffusion gradient directions within 44 h of scanning time. Based on the reconstructed SRR-DTI maps, whole brain probabilistic Track Density Imaging (TDI) was performed for the purpose of super resolved track density imaging, further pushing the resolution up to 40 μm isotropic. The DTI and TDI maps realized atlas-quality anatomical maps that enable a clear delineation of most components of the song control and auditory systems. In conclusion, this study paves the way for longitudinal *in vivo* and high-resolution *ex vivo* experiments aimed at disentangling neuroplastic events that characterize the critical period for vocal learning in zebra finch ontogeny.

Abbreviations: AD, axial diffusivity; ANTs, advanced normalization tools; b_0, non-diffusion weighted image; CC-TD, color-coded track density (map); CM, caudal mesopallium; DLM, medial part of the dorsolateral nucleus of the anterior thalamus; DMA, dorsomedial nucleus of the anterior thalamus; DTI, diffusion tensor imaging; DW, diffusion-weighted; EPI, echo planar imaging; FA, fractional anisotropy; fODF, fiber orientation distribution function; FOV, field of view; FPL, fasciculus prosencephalis lateralis; FWE, family wise error; FWHM, full width at half maximum; HVC, high vocal center (now used as proper name); Ico, intercollicular nucleus; LaM, lamina mesopallialis; LFS, lamina frontalis superior; LMAN, lateral magnocellular nucleus of the anterior nidopallium; MD, mean diffusivity; MLd, dorsal part of the lateral mesencephalic nucleus; MRI, magnetic resonance imaging; NCL, caudolateral nidopallium; NCM, caudomedial nidopallium; nXIIts, tracheosyringeal nucleus; OM, (tractus) occipitomesencephalicus; RA, robust nucleus of the arcopallium; RD, radial diffusivity; ROI, region of interest; SE, spin-echo; SE-EPI, spin-echo echo planar imaging; SNR, signal-to-noise ratio; SPM, statistical parametric mapping; SRR-b_0, super-resolution reconstruction b_0; SRR-DTI, super-resolution reconstruction diffusion tensor imaging; SRR-FA, super-resolution reconstruction fractional anisotropy; SRR-MD, super-resolution reconstruction mean diffusion; TeO, tectum opticum; TD, track density (map); TDI, track density imaging.

* Corresponding author. Present and permanent address: Bio-Imaging Campus Drie Eiken, UC 109, University of Antwerp, Universiteitsplein 1, 2610 Wilrijk, Belgium.
E-mail address: annemie.vanderlinden@uantwerpen.be (A. Van der Linden).

http://dx.doi.org/10.1016/j.neuroimage.2016.09.067
Received 27 May 2016; Accepted 29 September 2016
Available online xxxx
1053-8119/

1. Introduction

Songbirds – zebra finches in particular – are currently regarded as the best animal model available to study specific aspects of the neurobiology of human speech learning (Brainard and Doupe, 2013; Doupe and Kuhl, 1999). However, so far, no studies reported using non-invasive imaging methods to study the structural properties of the zebra finch brain *in vivo*. This strongly interferes with performing longitudinal studies aimed at tracing neuroplastic events along the process of vocal learning, establishing causal relationships between experience and brain plasticity and conducting whole-brain analyses. Previously, *in vivo* Diffusion Tensor Imaging (DTI) was successfully used in European starlings *(Sturnus vulgaris)* (De Groof et al., 2006) where De Groof et al. showed seasonally recurring neuroplastic changes in living songbirds (De Groof et al., 2009, 2008). These studies also showed that DTI is the MR method of choice to explore the anatomy of the songbird brain as conventional T1- and T2-weighted sequences do not yield anatomical contrast in the song control system (Van der Linden et al., 1998; Verhoye et al., 1998). However, the protocol used to image adult starlings across seasons cannot be used to obtain data of the zebra finch brain as the total scanning time was 8 hours to scan one hemisphere. Such extended acquisition times might interfere with studying structural brain changes related to the process of vocal learning in juvenile songbirds in a longitudinal study design. In addition, obtaining data from one hemisphere hampers the investigation of possible lateralization of effects (Toga and Thompson, 2003). Fortunately, in recent years, faster sequences have become available. Consequently, the first aim of this study was to implement an *in vivo* imaging protocol to acquire DTI data of the zebra finch brain in a shorter time frame (< 2 h).

The organization of the songbird brain is fundamentally different from the mammalian brain (Doupe and Kuhl, 1999; Jarvis, 2004; Jarvis et al., 2005). Instead of being organized in a multi-layered cortex as is the case in mammals, evolutionary similar pallium-derived structures are condensed in nuclei situated mainly in the forebrain (Karten and Shimizu, 1989). Fiber tracts connect distinct nuclei to subsequent relay stations. This modular arrangement results in extensive circuitries and is morphologically comparable to more ventrally situated brain areas in the mammalian brain such as the thalamus and basal ganglia. Two main pathways, together termed as the 'song control system', characterize the neural substrate encoding singing behavior (*i.e.* the anterior forebrain pathway and the caudal motor pathway). The first is most important in song learning (Aronov et al., 2008; Bottjer et al., 1984; Brainard and Doupe, 2000; Ölveczky et al., 2005; Scharff and Nottebohm, 1991) and consists of High Vocal Center (HVC) that sends projections to Area X which in turn projects to the medial part of the dorsolateral nucleus of the anterior thalamus (DLM) that contacts the lateral magnocellular nucleus of the nidopallium (LMAN) and finally reaches in the robust nucleus of the arcopallium (RA). The second pathway is responsible for the motor aspect of singing (Wild, 1997), encodes specific learned features of songs (Simpson and Vicario, 1990; Yu and Margoliash, 1996), and contains a direct projection from HVC to RA and then projects further downstream to the vocal organ via several tracts among which the tractus occipitomesencephalicus (OM) (Wild, 1993). Interestingly, only male zebra finches sing, consequently, the song control system is more enhanced in males. This sex difference in behavior was first discovered by Nottebohm and Arnold (1976a, 1976b) who reported dramatic volume differences between both sexes in Area X, HVC and RA, in canaries and zebra finches. From then onwards, several studies have explored the existence of sex differences in microstructural tissue properties describing differences in soma size (Nixdorf-Bergweiler, 2001), dendritic arborization (Gurney, 1981), distribution of perineuronal nets (Cornez et al., 2015; Meyer et al., 2014), often affecting only specific components of the song control circuitry. As structural sexual dimorphisms in the songbird have been described extensively in literature (Ball and Macdougall-Shackleton, 2001), this provides the ideal question to test the sensitivity of the optimized *in vivo* DTI protocol. In addition, as sex differences in the songbird brain are well characterized by histology, specific biological properties might be linked to the DTI parameter readout.

Despite the clear sex differences, so far only atlases of the male zebra finch brain are available (Karten et al., 2013; Nixdorf-Bergweiler and Bischof, 2007; Poirier et al., 2008). Hence, to obtain a high-resolution overview of the sex differences in the adult zebra finch brain, *ex vivo* imaging of a male and female brain was performed. To realize high-resolution DTI data within a shorter acquisition time, a recently developed super-resolution reconstruction (SRR) method (Van Steenkiste et al., 2016) was combined with super-resolved track density imaging (Calamante et al., 2010).

The aim of the current study was twofold: (1) to test a recently optimized *in vivo* DTI protocol to detect structural sex differences in the adult zebra finch brain, and (2) to perform *ex vivo* SRR-DTI scans on a male and female brain to obtain a clear, high-resolution view on the 3-dimensional organization of the adult zebra finch brain and to clarify specific findings detected in the *in vivo* data.

2. Materials and methods

2.1. Animals and ethical statement

Adult male and female zebra finches (*Taeniopygia guttata*; n=17/sex) were purchased at a local supplier or bred in the animal facility (birds older than 200 days post hatching were considered adult). The birds were kept in indoor aviaries in non-breeding conditions with food and water available *ad libitum*. All experimental procedures were in accordance with the European Directive 2010/63/EU and approved by the Committee on Animal Care and Use at the University of Antwerp, Belgium (permit number 2012-43).

2.2. Acquisition

2.2.1. In vivo *DTI*

The birds were anaesthetized with isoflurane (IsoFlo®, Abbott, Illinois, USA; induction: 2.5%; maintenance: 1.5–1.8%) in a mixture of 70% N_2O and 30% O_2 at a flow rate of 600 ml/min. Throughout the entire imaging protocol, the physiological condition of the animals was continuously monitored by means of a pressure sensitive pad to detect the breathing rate, and a cloacal thermistor probe to measure body temperature (MR-compatible Small Animal Monitoring and Gating system, SA Instruments, Inc.). The latter was connected to a tightly controlled warm air feedback system to maintain the birds' body temperature within narrow physiological ranges (40.0 ± 0.2) °C. All zebra finches recovered perfectly within a few minutes after the experiment.

Images were acquired on a 7 T horizontal MR system (PharmaScan 70/16 US, Bruker BioSpin GmbH, Germany) equipped with standard Bruker setup (*i.e.* a quadrature transmit volume coil, a linear array receive coil designed for mice and a 400 mT/m gradient insert (Bruker BioSpin, Germany)). First, Turbo RARE T_2-weighted pilot scans along three orthogonal directions were acquired to assess the birds' position. Second, a field map was acquired to measure magnetic field inhomogeneities after which local shimming was performed. Next, coronal diffusion-weighted (DW) four shot SE-EPI images were acquired with 60 optimally distributed diffusion gradient directions (Jones et al., 1999). Twenty-one non-DW b_0 data sets (b=0 s/mm²; 7 b_0 per 20 DW images) were acquired. The image parameters were: FOV (20×15) mm^2, TE 22 ms, TR 7000 ms, acquisition matrix (105×79), in-plane resolution (0.19×0.19) mm², slice thickness 0.24 mm, b-value 670 s/mm², diffusion gradient duration (δ) 4 ms, diffusion gradient separation (Δ) 12 ms, scan duration approximately 1 h 20 min. For practical reasons, the Field-of-View (FOV) was limited to the birds' telencepha-

lon, cerebellum and the major dorsal parts of the mesencephalon and diencephalon, since these brain areas contain most relevant auditory and song control system nuclei. The entire DTI protocol was repeated twice to increase the SNR. Immediately after DTI, a 3-dimensional (3D) RARE scan positioned identical to the DTI data set was acquired for registration purposes. Over the course of the experiment two similar RARE sequences were used (imaging parameters RARE^{A}: TE 11 ms (TE_{eff} 44 ms), TR 3000 ms, RARE factor 8, FOV (16×14×14) mm³, matrix (256×92×64), spatial resolution (0.06×0.15×0.22) mm³ zerofilled to (0.06×0.05×0.05) mm³, scan duration 35 min; or RARE^{B}: TE 11 ms (TE_{eff} 55 ms), TR 2500 ms, RARE factor 8, FOV (18×16×10) mm³, matrix (265×92×64), spatial resolution (0.07×0.17×0.16) mm³ zerofilled to (0.07×0.07×0.07) mm³, scan duration 29 min). Each imaging session took approximately 2 h 45 min.

2.2.2. Ex vivo *SRR-DTI*

Two adult males and one adult female zebra finch that took part in the *in vivo* study, were euthanized by an intramuscular injection of pentobarbital (Nembutal, Ceva Sante Animale; 60 mg/kg) and transcardially perfused with ice-cold 4% paraformaldehyde (PFA) in a 0.1 M Phosphate Buffered Saline (PBS; pH 7.4) solution supplemented with gadolinium (1% Dotarem, 0.5 mmol gadoteric acid/ml; Guerbet, France). Next, the brains were post-fixed overnight with 4% PFA in 0.1 M PBS enriched with 1% Dotarem after which the tissue was transferred to 0.1 M PBS with 1% Dotarem and kept at 4 °C for storage. The brains remained in the skull during the entire procedure so as to prevent mechanical damage throughout the different tissue processing and imaging steps.

Approximately eight hours prior to *ex vivo* imaging, the samples were removed from the refrigerator in order to acclimatize to the ambient bore temperature. The three zebra finch heads were imaged with a DW SE sequence on a horizontal 9.4 T MRI system (BioSpec, Bruker Biospin GmbH, Germany) with a circular polarized transmit resonator, quadrature receive surface coil and a 600 mT/m gradient insert (Bruker BioSpin, Germany). For one male and one female brain twelve low resolution data sets were acquired where each set was rotated around the phase-encoding direction at incremental steps of 15° for the purpose of super resolution reconstruction (Fig. 1). Each of these sets consisted of 1 b_0 and 5 DW images (b=2500 s/mm²) with following acquisition parameters: FOV (15×15) mm², TE 26 ms, TR 10 000 ms, acquisition matrix (192×137) zero-filled to (192×192), in-plane resolution of (0.078×0.078) mm², slice thickness 0.32 mm, 37 slices, δ 6 ms, Δ 14 ms, acquisition time 2 h 40 min. The test male sample underwent a slightly different imaging protocol, where instead of 12 sets of low resolution images, 15 low resolution data sets were acquired rotated around the phase encoding axis at incremental steps of 12°. In addition, for each low resolution acquisition angle, 1 b_0 image together with 6 DW scans were acquired. All other imaging parameters remained identical. For each slice orientation, the diffusion gradient directions were uniformly sampled based on a method proposed by (Caruyer et al., 2013). The in total 60 (male and female) or 90 (test male) diffusion gradient directions were selected and programmed in the absolute x-y-z coordinate system of the scanner. For details on the theory supporting the super-resolution reconstruction acquisition protocol we refer to (Van Steenkiste et al., 2016). Total acquisition time was approximately 44 h (test sample) or 28 h (one male, one female) per sample.

2.3. Data processing

2.3.1. In vivo

First, the diffusion data were realigned to correct for subject motion using the Diffusion II toolbox in SPM8 (Statistical Parametric Mapping, http://www.fil.ion.ucl.ac.uk/spm/). First, a rigid registration was performed between the b_0 images which was followed by an extended registration taking all DW images into account.

The realigned DW-images of each subject were co-registered to the 3D RARE data set of the same imaging session using mutual information as the similarity metric. In parallel, the 3D RARE data set was spatially normalized to match the zebra finch atlas using a global 12-parameter affine transformation followed by nonlinear deformations. Next, the transformation matrix of the spatial normalization was applied to the realigned and co-registered DW images. Then, the diffusion tensor was estimated and DTI parameter maps were computed (*i.e.* fractional anisotropy (FA), mean diffusivity (MD), axial diffusivity (AD) and radial diffusivity (RD)). Finally, all DTI parameter maps were smoothed in plane using a Gaussian kernel (FWHM=0.3 mm×0.38 mm).

2.3.2. Ex vivo

2.3.2.1. DTI with super-resolution reconstruction (SRR-DTI). From the acquired low resolution DW images, high resolution diffusion tensors were estimated on a (0.078×0.078×0.078) mm^3 grid, using SRR-DTI (Van Steenkiste et al., 2016). SRR-DTI combines the DTI estimation with super-resolution reconstruction, thereby enabling the direct estimation of high resolution diffusion tensors from a set of low resolution DW images. The motion parameters used by SRR-DTI were estimated using an iterative model-based motion correction scheme (Bai and Alexander, 2008).

2.3.2.2. Super-resolved track density imaging (TDI). In order to obtain fiber orientation distribution functions (fODFs) suitable for probabilistic fiber tracking, the following steps were performed. First, a dense set of predicted high resolution DW images were obtained from the high resolution diffusion tensor parameters estimated using SRR-DTI. Next, the white matter fiber response function was extracted from the high resolution DW data using the recursive calibration method described in Tax et al. (2014). Finally, fODFs were obtained by performing constrained spherical deconvolution (Tournier et al., 2007), using the high resolution DW images and the single fiber response function created above, adopting the quadratic programming approach outlined in (Jeurissen et al., 2014). The spherical harmonic series describing the fODFs was terminated at order 8.

Probabilistic whole brain tractography was then performed using second order integration over the fODFs (Tournier, 2010). 10^8 streamlines were generated using the following parameters: fODF amplitude threshold of 0.1, step size of 0.08 mm, and a maximum angle between steps of 9°. From the resulting tractogram, track density maps were calculated at a super-resolution of (40×40×40) µm³ (Calamante et al., 2010). In addition, probabilistic seed-based tractography was also performed in the male and female data set using the same parameters to visualize fibers encapsulating Area X. All steps were performed using MRtrix version 0.3 (Tournier et al., 2012) (www.mrtrix.org).

2.4. Statistical analysis

A voxel-wise 2-sample *t*-test was used to test for differences between males and females for each DTI parameter map separately. To correct for multiple comparisons, a family-wise error (FWE) correction thresholded at $p < 0.05$ was applied. Besides this very stringent correction, all statistical parameter maps were assessed uncorrected with an arbitrary threshold at $p < 0.001$ in combination with a minimal cluster size of 3 voxels. The statistical maps were superimposed on the zebra finch atlas (displayed uncorrected $p < 0.01$; minimum 16 voxels).

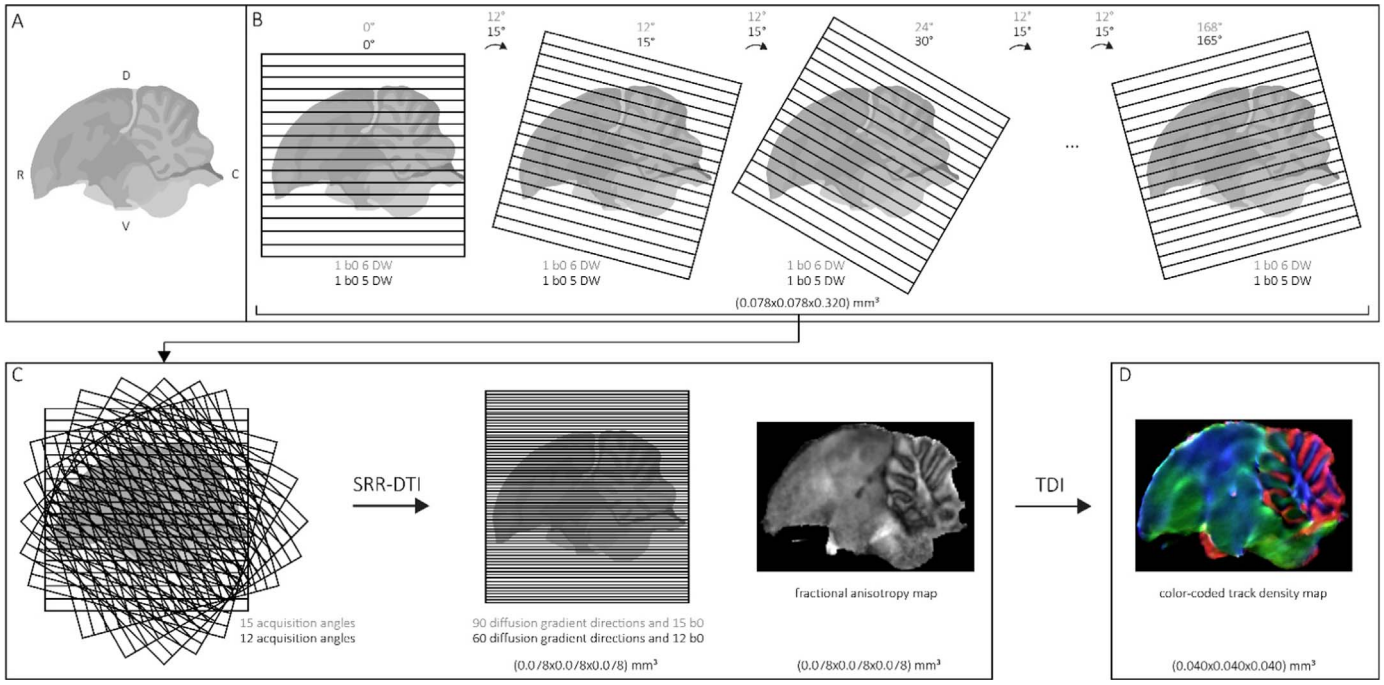

Fig. 1. Schematic overview of the SRR-DTI data acquisition protocol. (A) Sagittal view of the zebra finch brain. (B-C-D) Chronological overview of the scanning procedure illustrating the different low resolution data sets that are rotated at incremental steps of either 15° (male and female brain, black font) or 12° (test male brain, gray font) around the phase-encoding axis. (C) All low-resolution data sets are reconstructed into a high-resolution grid along which the diffusion tensor is estimated and the DTI parameter maps are calculated. (D) Based on the reconstructed high-resolution SRR-DTI data, whole-brain fiber tractography was performed which resulted in track density images. Abbreviations: R: rostral; C: caudal; D: dorsal; V: ventral.

3. Results

3.1. In vivo *DTI*

Independent voxel-wise two-sample t-tests comparing male and female DTI parameter maps revealed significant differences in several DTI parameters at various locations in the brain. As expected from a behavioral point of view (only males sing), most differences could be co-localized with the song control system nuclei. When investigating the statistical maps using an arbitrary threshold (no FWE correction), significant clusters complementary to the FWE findings could be observed. A detailed overview of the voxel-based results can be found in Table 1.

3.1.1. *Fractional anisotropy*

The strongest difference between adult male and female zebra finches was found bilaterally in the tissue surrounding Area X (Left: $p < 0.001$; Right $p=0.023$; FWE corrected), a part of the anterior forebrain pathway involved in song learning. Within this cluster FA values are higher in males as compared to females. Close examination of the cluster suggests that it is situated mainly at the dorso-caudo-lateral edge almost entirely encapsulating Area X (Fig. 2A). In addition,

Table 1
Summary of the results of the voxel-based analysis comparing male to female DTI parameter maps.

	M > F					M < F				
	brain area	hemisphere	cluster size[a]	p	p[b]	brain area	hemisphere	cluster size[a]	p	p[b]
FA	Area X surroundings	Left	215	< 0.001	$< 0.1*10^{-07}$	HVC	Left	28	0.004	$1.59*10^{-07}$
				0.009						
		Right	44	0.023	$< 0.1*10^{-05}$		Right	29	0.004	$1.73*10^{-07}$
			26	0.043	$< 0.1*10^{-04}$					
	part of tractus OM	Left	5		$1.97*10^{-04}$					
		Right	10		$2.63*10^{-04}$					
MD	HVC	Left	14	0.009	$1.88*10^{-07}$					
		Right	3		0.001					
	LMAN	Left	17		$2.47*10^{-06}$					
		Right	3		$4.17*10^{-04}$					
AD	HVC	Left	5		$2.77*10^{-06}$					
	LMAN	Left	8		$4.76*10^{-05}$					
RD	HVC	Left	19	0.004	$6.35*10^{-08}$					
		Right	8		$2.04*10^{-04}$					
	LMAN	Left	17	0.022	$1.21*10^{-06}$					
		Right	9		$1.12*10^{-04}$					
	RA	Right	6		$8.69*10^{-05}$					

p and p[b]: p-value at peak level of the cluster.

[a] Cluster size: number of voxels in cluster when significance level is set uncorrected $p < 0.001$.
[b] Not corrected for multiple comparisons.

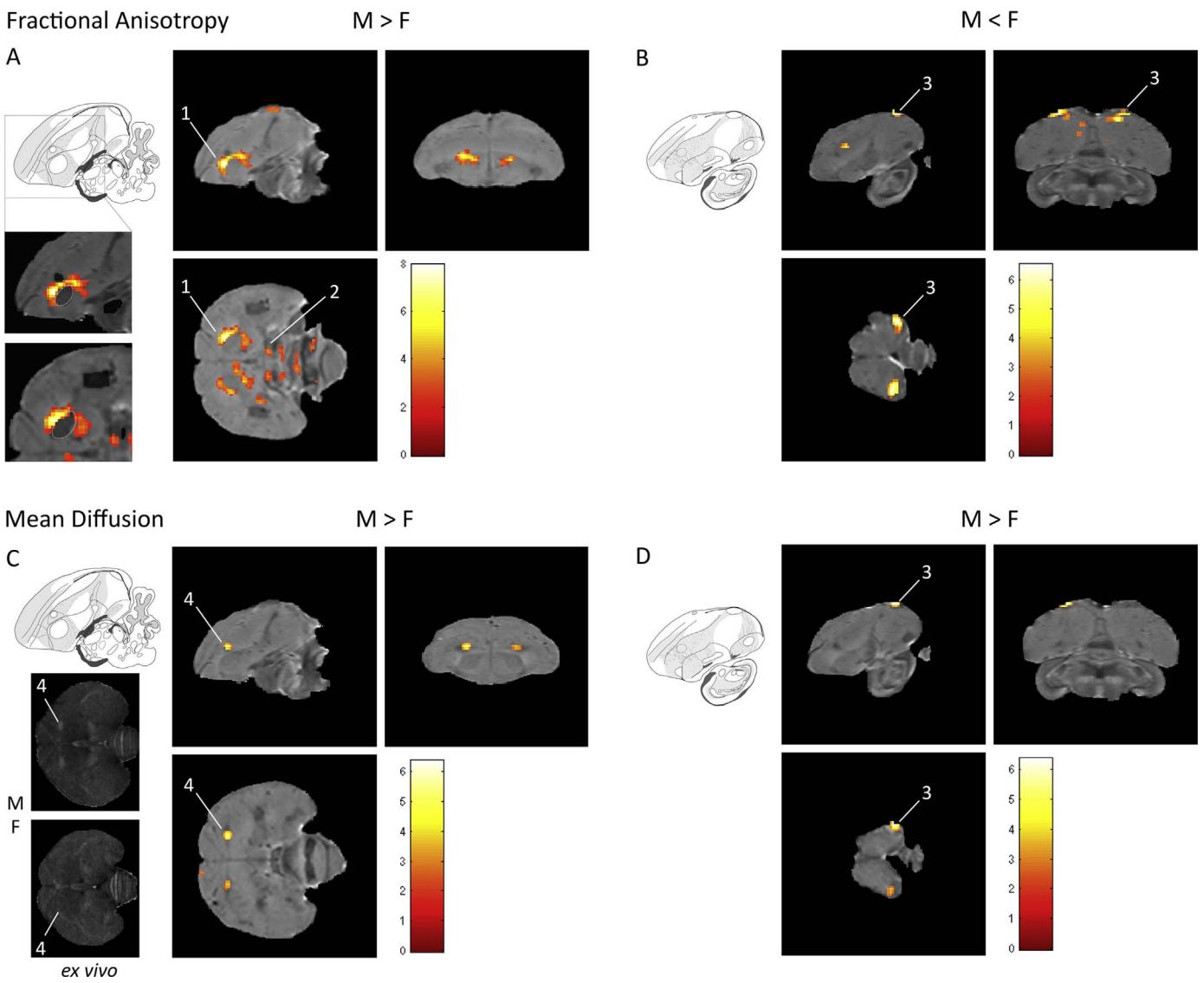

Fig. 2. *In vivo* DTI confirms known sex differences. Statistical maps showing the voxels where (A) FA values are higher in males compared to females, (B) FA values are smaller in males compared to females, or (C)–(D) MD values are higher in males compared to female zebra finches. The statistical results are displayed uncorrected $p < 0.01$ and overlaid onto the ZF atlas (Poirier et al., 2008). The t-values are color coded according to the scales displayed on the right side of each panel. The numbers represent: (1) Area X surroundings, (2) part of *the tractus OM*, (3) HVC and (4) LMAN. The sagittal schematic atlas drawings are obtained from the zebra finch histological atlas browser (Karten et al., 2013), with permission of John Wiley and Sons. Both MRI inserts in panel A display a sagittal (top) and horizontal (bottom) slice of the *ex vivo* MRI atlas and illustrate that the cluster encapsulates Area X which is delineated by a white line. The two insets in panel C are the *ex vivo* SRR-MD maps of the male (top) and female (bottom) sample. LMAN (4) can be seen as hyperintense spots on the male data set, whereas it cannot be discriminated from the surrounding tissue on the female data set.

a small part of the tractus OM rostral to nucleus DLM showed up as well (Left: p=0.0002 (5 voxels); Right: p=0.0003 (10 voxels); uncorrected; Fig. 2A).

FA values were higher in females as compared to males in two clusters at the location of HVC (Left: $p < 0.004$; Right $p < 0.004$; FWE corrected; Fig. 2B). When lowering the threshold for visualization of the statistical result to $p < 0.01$, the clusters extend ventro-medially towards the dorsal part of NCM and Field L (Fig. 2B).

3.1.2. Mean diffusivity

A significantly increased MD in males compared to females was observed in left HVC (p=0.009; FWE corrected). When exploring the data set without multiple comparison correction also right HVC (p=0.001; uncorrected) and LMAN (Left: $p < 0.001$; Right: $p < 0.001$; uncorrected) were found to be different (Fig. 2C–D). The latter cluster can be visually confirmed on the *ex vivo* data sets as a hyperintense spot covering LMAN in the male but not the female MD maps (inset Fig. 2C). There were no areas found which displayed a higher MD in females as compared to males.

3.1.3. Axial diffusivity

After multiple comparison correction, no clusters demonstrating a sex difference in AD could be found. When lowering the statistical threshold to $p < 0.001$ uncorrected, left HVC and left LMAN were found to have higher AD in males ($p=2.77*10^{-06}$; $p=4.76*10^{-05}$ respectively). After exploring the statistical maps with $p < 0.01$, both contralateral HVC and LMAN were found to be different as well. Moreover, two clusters with great resemblance to the Area X surroundings – similar to the voxel-wise difference in FA – were detected (Left and Right: p=0.001). No other differences in AD have been observed.

3.1.4. Radial diffusivity

Both left LMAN and left HVC were found to have a significantly higher RD in males as compared to females (p=0.022; p=0.004; FWE corrected). Without multiple comparison correction the contralateral LMAN and HVC also displayed a clear disparity in RD ($p=2.04*10^{-04}$;

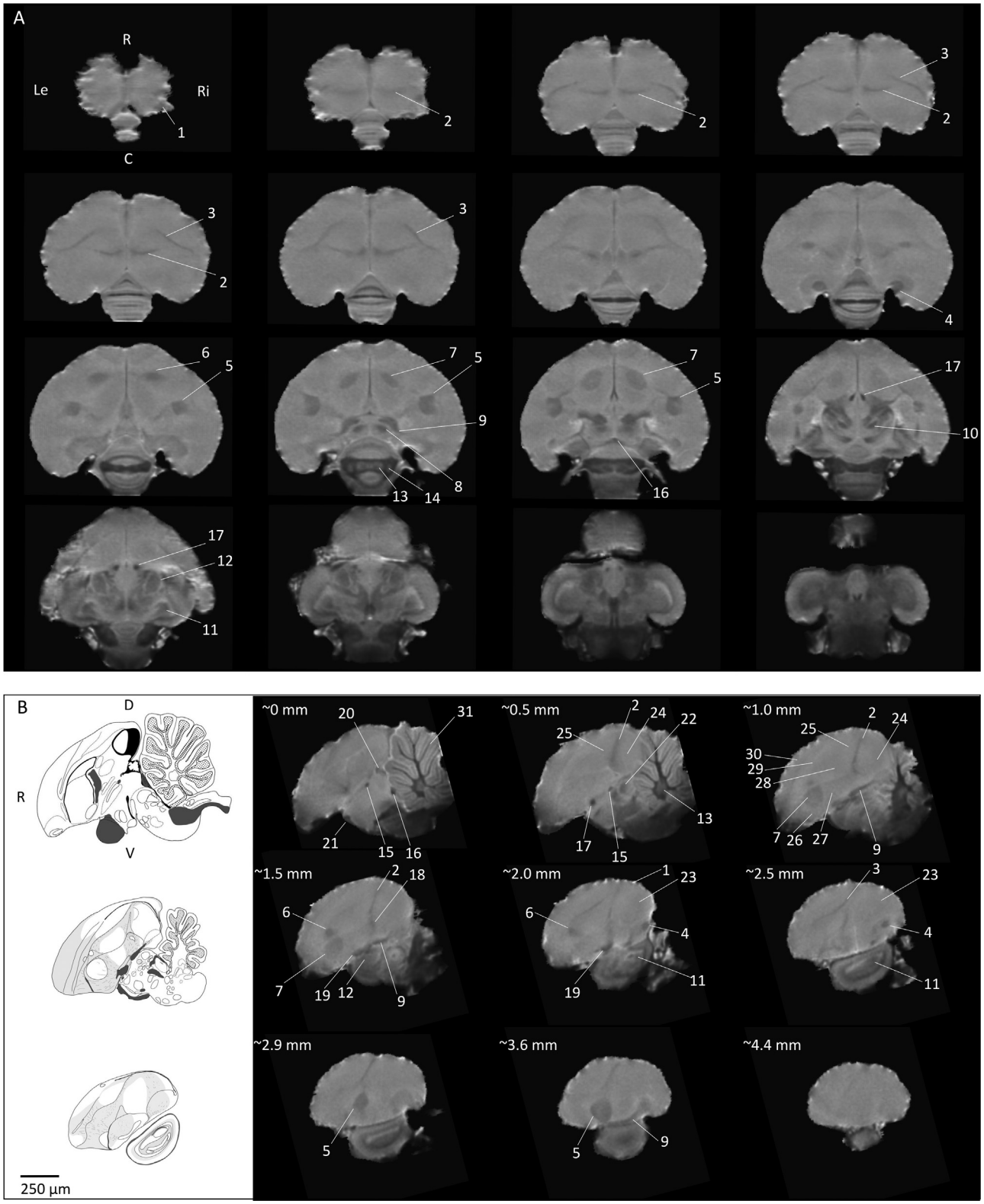

Fig. 3. Overview of anatomical contrast provided by the male *ex vivo* SRR-DTI b_0 data set. Consecutive slices are ordered from left to right where the top left slice represents the most dorsal or medial and the bottom right slice the most ventral or lateral part of the zebra finch brain for respectively the horizontal or sagittal images. The schematic atlas drawings correspond to the adjacent sagittal MR image. For each sagittal slice the approximate distance from the midline is specified. The following structures can be identified: (1) HVC, (2) Field L, (3) lamina mesopallialis, (4) nucleus robustus arcopallialis, (5) entopallium, (6) LMAN, (7) Area X, (8) DLM, (9) tractus occipitomesencephalicus, (10) nucleus ovoidalis, (11) MLd-DM-Ico (intercollicular nucleus) complex, (12) nucleus rotundus, (13) medial cerebellar nucleus, (14) lateral cerebellar nucleus, (15) commissura anterior, (16) commissura posterior, (17) tractus septomesencephalicus, (18) globus pallidus, (19) fasciculus prosencephalis lateralis (FPL), (20) plexus choroidalis, (21) chiasma opticum, (22) DMA, (23) NCL, (24) NCM, (25) CM, (26) striatum mediale, (27) striatum, (28) nidopallium, (29) mesopallium, (30) hyperpallium, (31) cerebellum. Abbreviations: (R) rostral, (C) caudal, (D) dorsal, (V) ventral, (Le) left, (Ri) right. The sagittal schematic atlas drawings are obtained from the zebra finch histological atlas browser (Karten et al., 2013), with permission of John Wiley and Sons.

p=1.12*10^{-04}, respectively), interestingly, a small cluster near right nucleus RA was detected as well (p=8.69*10^{-05} uncorrected).

3.2. Ex vivo *SRR-DTI and TDI*

The SRR-DTI protocol resulted in high quality diffusion MRI data, which were reconstructed into one data set characterized by an isotropic resolution of 80 µm. The different DTI parameter maps show a clear anatomical contrast. The implementation of the SRR technique to acquire DTI data resulted in a significant reduction of the total acquisition time (*i.e.* ± 28 h or ± 44 h for respectively 60 or 90 diffusion gradient directions). Other studies that use high-resolution *ex vivo* DTI, report on long acquisition durations, or reduce the angular and/or spatial resolution to obtain reasonable acquisition times. This marked reduction in scanning time also extends to T_2-weighted anatomical 3-dimensional data sets. If only the b_0 images would have been acquired, the total acquisition time would be approximately 4.67 h or 6.29 h. This is in line with Poot et al. (2010).

3.2.1. *Neuroanatomy*

For all visualizations, the same reference frame as the *ex vivo* zebra finch atlas (Poirier et al., 2008) was chosen (*i.e.* the symmetrical axis of the brain and a 10° clockwise rotation compared to the base of the brain in the midsagittal slice). This closely matches aligning the commissura anterior and posterior in a horizontal plane on the midsagittal slice.

Fig. 3 provides an overview of the different anatomical structures visible on the male SRR-b_0 data set. Many similarities can be found with the recently published schematic drawings by Karten and Mitra (www.brainarchitecture.org; (Karten et al., 2013); Fig. 3b). Interestingly, several components of the song control circuitry (*i.e.* HVC, RA, LMAN, Area X and DLM), auditory system (*i.e.* MLd, nucleus ovoidalis, Field L), visual system (*i.e.* entopallium and nucleus rotundus) can be identified. In addition, many tracts that connect different brain areas can be localized as well. For example, the tractus OM which is a tract connecting the caudal motor pathway (HVC-RA) to the tracheosyringeal nucleus (nXIIts), and the chiasma opticum which contains the tractus opticus that relays information from the eyes to the tectum opticum can all be discerned.

The brain samples scanned for the SRR-b_0 and the *ex vivo* atlas (Poirier et al., 2008) were processed identically (*i.e.* perfused with 4% PFA and 1% Dotarem), and both imaging protocols resulted in the same spatial resolution. Consequently, when comparing the SRR-b_0 images of the male zebra finch to the *ex vivo* zebra finch atlas (Poirier et al., 2008), the resulting anatomical contrast is very similar. However, some differences can be observed (Fig. 4). First, the SRR-b_0 images yield some additional contrast near the cerebellum enabling the identification of the different cerebellar layers (*i.e.* molecular and Purkinje-granule cell layers, the latter two cannot be distinguished on the SRR-b_0 data sets). Second, the boundaries of Area X are more clearly visible on the SRR-b_0 image compared to the *ex vivo* atlas. HVC, on the other hand, is more clearly visible on the *ex vivo* atlas. Lastly, the SRR-b_0 images more closely resemble the *in vivo* 3D RARE data (data not shown).

Visual inspection of the male and female SRR-b_0 data sets clearly shows the sex difference in Area X, RA and HVC (Fig. 5). While in general smaller in females compared to males (Nottebohm and Arnold, 1976a), HVC and RA cannot be differentiated from the surrounding tissue in the female SRR-b_0 data set. All other components of the song control circuitry (*e.g.* LMAN and DLM), and other systems, are clearly discernable in both sexes. Given that the SRR-b_0 of the male data set achieves the same anatomical contrast as the *ex vivo* atlas, the female SRR-b_0 data set can serve as the first female zebra finch atlas.

3.2.2. *Tractography*

Overall, TDI and seed-based tractography markedly complement the T_2-weighted data set by providing 3-dimensional anatomical information on the macroscale structural connectivity of the songbird brain (Fig. 6).

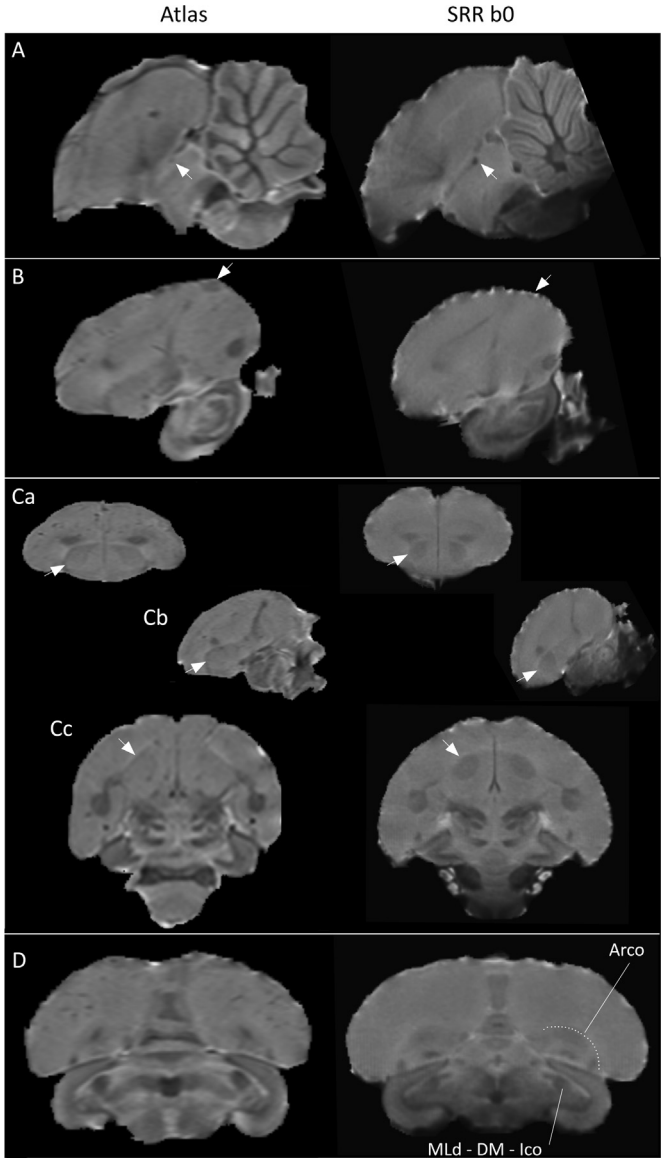

Fig. 4. Comparison of the *ex vivo* zebra finch atlas by Poirier et al. (2008; left) and the *ex vivo* SRR-b_0 of a male zebra finch (right). In general, the same anatomical information can be extracted from both data sets. A few exceptions can be found. A: The commissura anterior (arrow) is more difficult to localize on the midsagittal slice on the *ex vivo* atlas compared to the SRR-b_0 image. Panel B shows that HVC is more clearly visible on the *ex vivo* atlas compared to the SRR-b_0. C: Area X is vaguely visible on the *ex vivo* atlas compared to the SRR-b_0, especially on the sagittal and horizontal slices (Cb and Cc respectively). Panel D illustrates that the SRR-b_0 image yields addition anatomical contrast near the arcopallium (Arco), and MLd-DM-Ico complex.

3.2.2.1. TDI. TDI generated TD maps characterized by an additional increase in spatial resolution (40×40×40) µm³ by using a subvoxel fiber tracking procedure similar to Calamante et al. (2010). The signal intensity and color-code of the TD maps informs on respectively the number and orientation of fibers estimated by the fiber tracking procedure. In contrast to FA, the resulting TD maps allow a very clear delineation of different brain areas (Figs. 6–8) and provide clear anatomical contrast on general subdivisions of the brain (Fig. 8).

Anatomical structures that show a similar signal intensity on FA maps or appear as one structure on myelin stained brain slices, can be

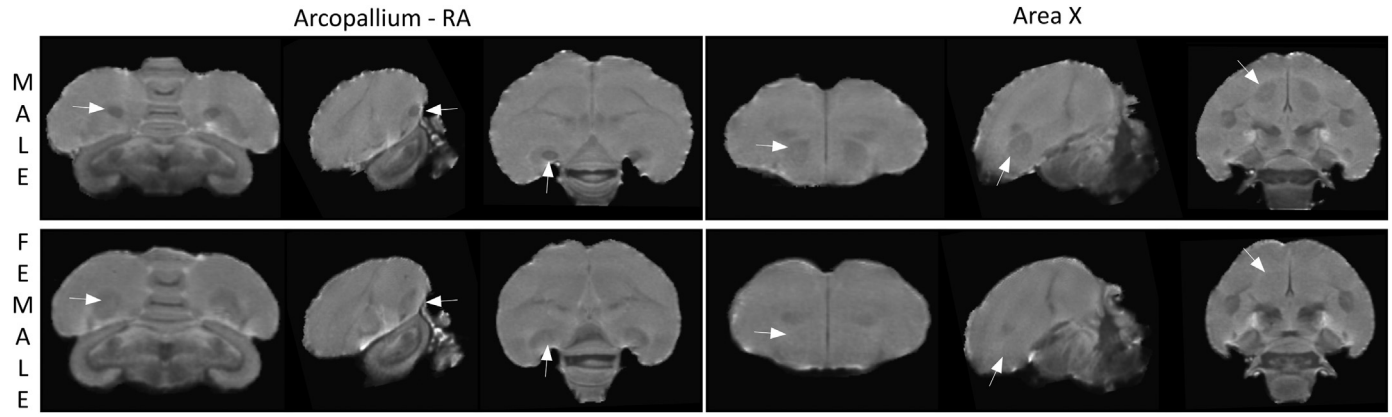

Fig. 5. Sex difference near RA and Area X visualized by the *ex vivo* SRR-b_0. Male and female images can be found on the top and bottom row respectively. The left panel shows that nucleus RA can be clearly seen on the male data set, whereas it is not noticeable in the female brain. The same accounts for the right panel. Area X (arrow) can be demarcated clearly on the male images, whereas it cannot be identified in the female brain.

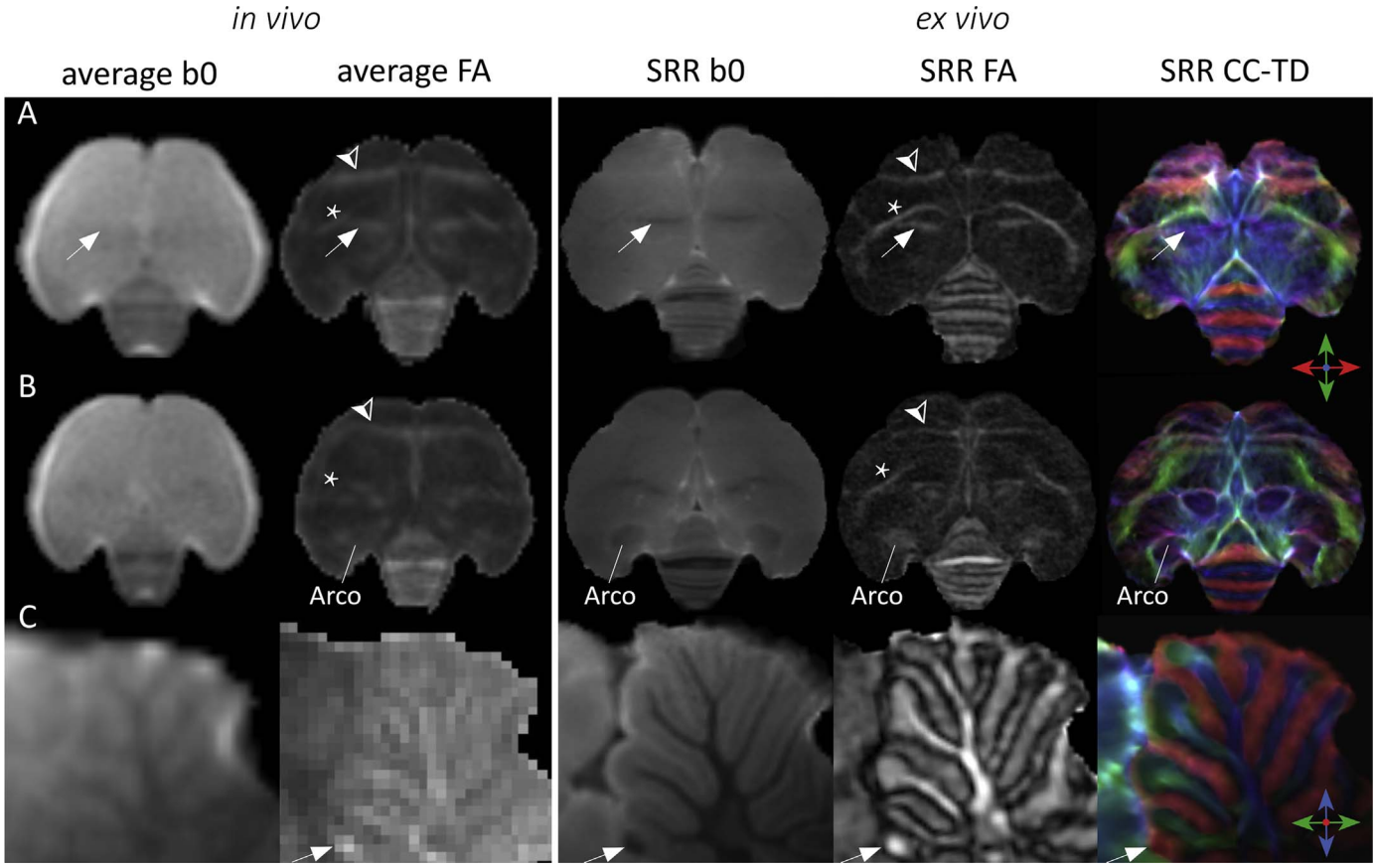

Fig. 6. Visual comparison of the different modalities derived from the *in vivo* DTI and *ex vivo* SRR-DTI acquisition of the female brain. The three different modalities are presented in the different columns: average b0 image of 17 female birds (left image *in vivo* panel), average FA of 17 female birds (right image *in vivo* panel), SRR-b_0 (left image *ex vivo* panel), SRR-FA (middle image *ex vivo* panel) and SRR color-coded track density (CC-TD) maps (right image *ex vivo* panel). The three rows represent distinct locations in the brain: (A) horizontal slice through Field L (arrow), *lamina mesopallialis* (LaM, *) and *lamina frontalis superior* (LFS, arrow head), (B) horizontal slice through the *arcopallium* (Arco), LaM (*) and LFS (arrow head), (C) midsagittal slice focused on the cerebellum and *commissura posterior* (arrow).

further subdivided and specified on the color-coded TD maps. This is illustrated in Fig. 6A. For example, Field L and the LaM appear very similar on the FA map, whereas on the SRR CC-TD map they are represented in different colors that indicate the difference in directionality of both fiber-containing structures. This characteristic also helps to differentiate between distinct brain structures near the met-, mes- and diencephalon (Figs. 7 and 8).

3.2.2.2. Seed-based tractography. The voxel-based comparison on the male and female FA maps shows a clear cup-shaped bilateral cluster encapsulating Area X (Fig. 2A). Based on the location and shape of the cluster and based on the fact that only a difference in FA was found, it is very likely that the observed disparity originates from a difference in fiber density or fiber organization, rather than a volumetric difference that has been described extensively by histology (Nottebohm and Arnold, 1976a). To further explore the precise nature of this difference, seed-based fiber tractography was performed. The result is shown in Fig. 9. A unilateral seed was placed in the center of Area X in the male brain and in the corresponding brain area in the striatum of the female brain. Even though both hemispheres were run

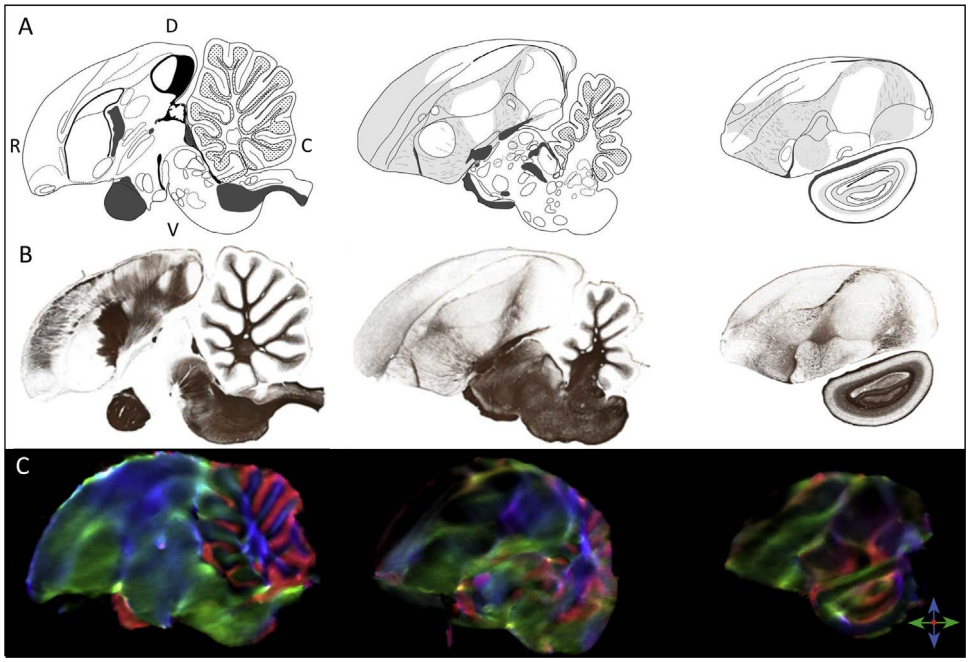

Fig. 7. Comparison of the SRR CC-TD maps of the test male to the schematic atlas drawings and myelin-stained tissue sections. Panel A-B-C allows to compare the *ex vivo* TD maps of panel C (test male) to corresponding publicly available myelin stained brain sections (B) and schematic atlas drawings (A) (Karten et al., 2013), reprinted with permission of John Wiley and Sons.

separately, the resulting streamlines display a very symmetrical path both in the male and the female data set. The male data shows that the fibers run around a central 'void' of which the location and shape show convincing similarities to the anatomy of Area X (Figs. 3–5 and 9). In contrast, the female data set demonstrates that the fibers originate and end very similar to the male, however, the streamlines appear to travel through instead of around Area X (or striatum).

Besides Area X, additional seeds were placed in other components of the song control and auditory system including LMAN, HVC, RA, MLd and Field L. The resulting streamlines show the immediate surroundings and the tract originating and/or arriving in the nuclei. It was not possible to visualize the entire song control circuitry, however, individual connections (*e.g.* X-DLM), were found. No left-right connectivity could be observed in any of the song control seeds tested. When placing a seed in nucleus rotundus, however, the estimated fibers ended up near the contralateral nucleus rotundus crossing the midline at the commissura posterior and, to a lesser extent, the commissura anterior (Fig. 10A–B).

4. Discussion

The present study demonstrates that (1) the *in vivo* DTI protocol is sensitive enough to detect structural disparities near Area X, HVC and LMAN, and extends current knowledge by showing a difference near the tractus OM, (2) the implementation of SRR-DTI in an *ex vivo* imaging protocol markedly reduced the acquisition time without interfering with spatial and angular resolution, (3) *ex vivo* SRR-DTI-based TDI provides an exquisite view on the structural connectivity of the adult male ànd female zebra finch brain and clarifies the difference in FA near Area X observed by *in vivo* DTI.

4.1. In vivo *detection of sex differences*

In general, most differences appeared bilateral. Therefore, we conclude that there is no clear cerebral asymmetry of sex differences. This is in line with the work of Nixdorf-Bergweiler (1996) who did not find left-right differences in the volumes of LMAN, HVC, RA and Area X as defined based on Nissl stainings (Nixdorf-Bergweiler, 1996).

4.1.1. Macrostructural differences in fiber organization

4.1.1.1. Area X surroundings. The strongest cluster detected in this *in vivo* study concerns a difference in FA in a cluster that encapsulates Area X. Interestingly, this observation matches previous reports: while being the largest song control nucleus in males (± 1.5 mm^3), Area X cannot be discerned at all in females (MacDougall-Shackleton and Ball, 1999; Nottebohm and Arnold, 1976b). To further clarify whether the observed cluster relates to a microstructural difference – Area X *versus* medial striatum in females– or reflects a marked contrast in fiber capsula surrounding Area X –similar to the RA cup, HVC shelf and entopallium belt regions– we performed *ex vivo* SRR-DTI and tractography (Figs. 9–10). In the male data set, the streamlines appear to delineate a structure of which the shape bears great resemblance to Area X. In females, on the other hand, the tracts run throughout the medial striatum. Interestingly however, both in the male and the female data set, the fibers appear to gather in the caudal part of the medial striatum to then travel caudally towards DLM, in the thalamus. This indicates that also in the female striatum –even in the absence of Area X– fibers gather and project in a manner similar to male zebra finches.

Apart from a clear anatomical difference visible on the *ex vivo* SRR-b_0 data sets, no differences in any other DTI parameter could be found in the tissue situated within Area X and the corresponding medial striatum in female birds. One could conclude that this *in vivo* DTI protocol is not sensitive enough to detect microstructural differences between Area X and the corresponding striatum in female birds. However, Person et al. (2008) described that even though there appears to be an extensive and highly specific topographic organization of neurons projecting from Area X and from the surrounding medial striatum to DLM, the morphology of the projecting cells is almost identical between both cell groups. Reiner et al. (2004) also report similarities in morphology of DLM projecting neurons whether they are located in Area X or in the surrounding striatum and describe them as having 'pallidal traits'. Therefore, if only subtle morphological differ-

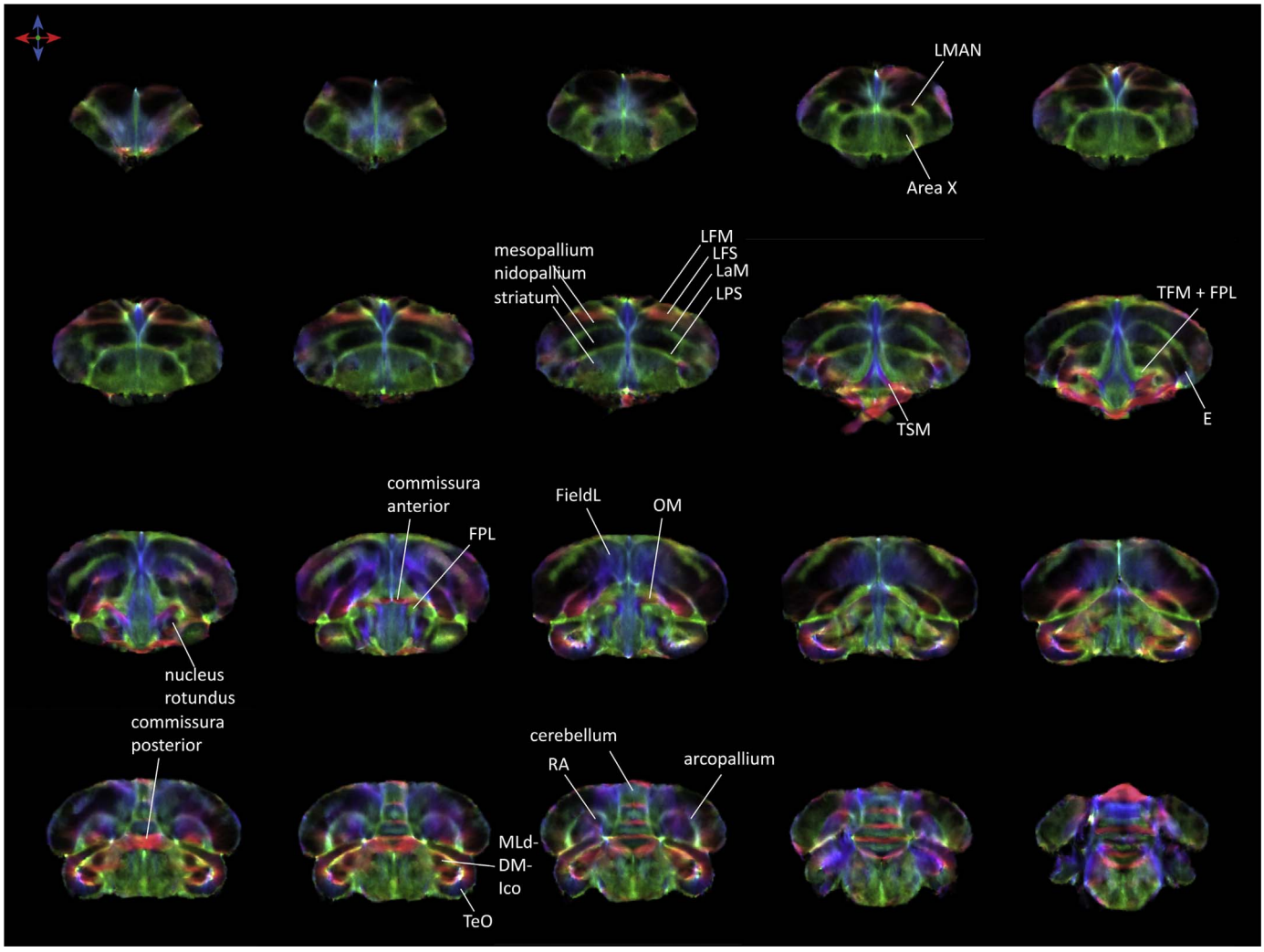

Fig. 8. Coronal overview of the SRR CC-TD maps of the test male. The TD maps provide a complementary anatomical contrast to Fig. 3. The TD maps allow to trace the connections between different components of *e.g.* the song control circuitry 3-dimensionally. In addition, several song control nuclei (*e.g.* LMAN and Area X) can be accurately demarcated based on the TD maps. Abbreviations can be found in the text, except for lamina pallio-subpallialis (LPS), tractus thalamo-frontalis and frontalis-thalamicus medialis (TFM), lamina frontalis suprema (LFM).

ences can be observed in cell populations within and outside of Area X in male birds, finding a difference between the medial striatum in female birds and Area X in males is, as a consequence, also less likely. Therefore, we conclude that the difference uncovered by *in vivo* DTI reflects a disparity in the (fiber) capsula surrounding Area X, which is absent in the female brain.

4.1.1.2. Parts of the tractus OM. We found an increased FA in males compared to females in the tractus OM rostral to DLM. This increase in FA in males might be indicative of a more densely organized or more robust tract in males compared to females. To our knowledge, this has never been reported before. This tract contains several fiber bundles that –among others– connect the caudal motor pathway (HVC-RA) to the syrinx, the avian analogue of the larynx (Wild, 1993). In recent years, more research has focused on the effects of brain plasticity in healthy adults and how physical training and/or cognitive experience can affect brain grey and white matter. For review we refer to Zatorre et al. (2012). Even though the difference described here is not found after correlation of the DTI parameters to a specific behavioral performance or after comparison of pre- and post-training imaging sessions, the clear behavioral dimorphism '*males sing and females do not*', implies that vocal practicing might also have repercussion on this very specific subpart of the vocal motor pathway.

4.1.2. Microstructural tissue characteristics

4.1.2.1. HVC. Even though HVC cannot be discerned on the T2-weighted 3D RARE and as a consequence possible size differences between different birds cannot be corrected for during the normalization procedure, the shape and location of the cluster suggests that the observed difference relates to a disparity in intrinsic cytoarchitectural properties rather than a macrostructural volume difference.

HVC was found to have a higher FA in females, compared to males. Interestingly, Nixdorf-Bergweiler and Von Bohlen und Halbach (2004) observed a strong male-biased (M > F) difference in the number of myelinated axonal profiles per unit area of tissue in adult zebra finches in HVC. Intuitively, one would expect that a higher density of axonal profiles is linked to a higher FA, however, this assumption only holds up if the axonal fibers are coherently organized (Mori and Zhang, 2006). Furthermore, part of the axonal profiles that originate in HVC travel to RA. The tract connecting HVC and RA is termed the caudal motor pathway owing to its role in the motor aspect of singing (Wild, 1997). Instead of being organized into a vast bundle of parallel fibers

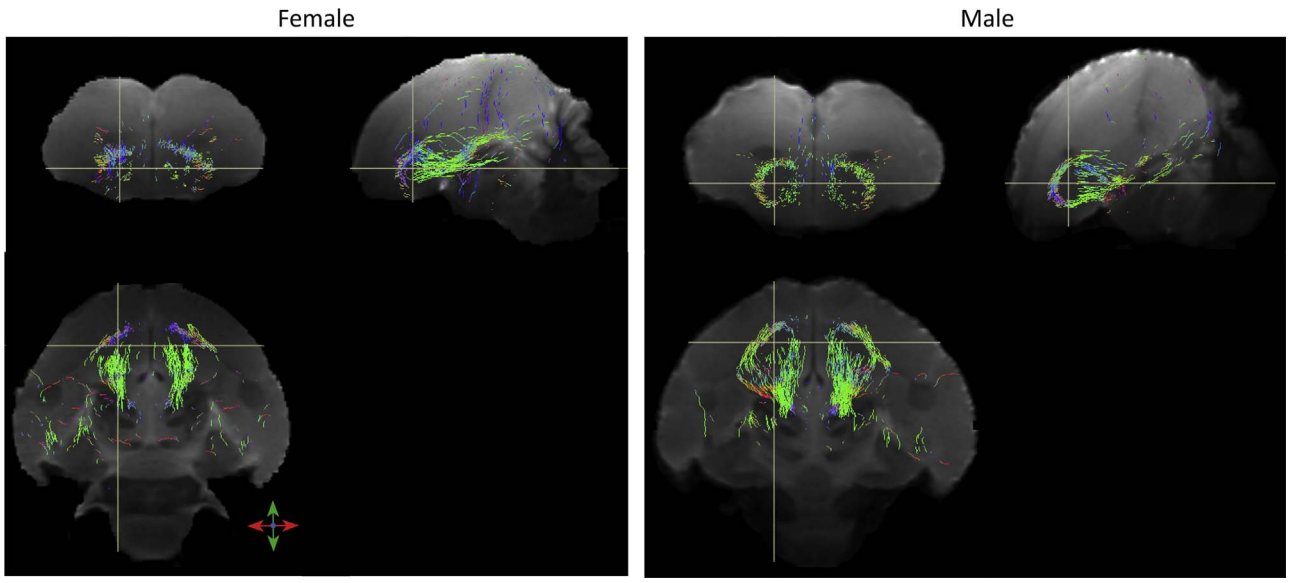

Fig. 9. Tractography clarifies the sex difference of Area X surroundings. Seed-based fiber tractography performed in the male (right) and female (left) zebra finch brain in MRtrix using the following parameters (seed placed in the center of Area X or corresponding coordinate in the medial striatum, sphere with radius of 1.0 mm, 500 tracks, angle 45°, minimum length 0.3124 mm, maximum length 150 mm, step size 0.04 mm). Both hemispheres were run separately and resulted in relatively symmetrical fiber populations (left *versus* right hemisphere). The cross-hair points to the approximate coordinates of the center of Area X or the corresponding location in the female striatum (location of seed). In the male data set, no fibers were estimated near the point where cross-hairs meet. Instead, they appear to demarcate an Area X-shaped void. The different fibers appear to converge near the dorsoventral border of Area X where they extend towards DLM. In contrast, fiber tracking in the female data set shows no clear demarcation of Area X.

similar to the European starling (De Groof et al., 2006), the zebra finches' caudal motor pathway consists of fibers that are almost individually projecting from HVC to RA (Karten et al., 2013). Its relatively 'diffuse' nature combined with the partial volume effect inherent to DTI makes it impossible to visualize the tract or detect any differences along its path, even though this sex difference has been described extensively in the literature (Konishi and Akutagawa, 1985; Mooney and Rao, 1994; Wang et al., 1999). Despite observing differences along the path, the FA cluster co-localized with HVC might suggest detecting a difference in fibers exiting HVC. In male birds, more myelinated axons leave HVC, but in a less well organized manner compared to female birds. This might be partly responsible for a lower FA in males compared to females.

Differences in the number of axonal profiles and RA-projecting axons are not likely to be solely accountable for the disparity observed in FA. Another possible candidate are interneurons. By investigating zebra finches, Grisham and Arnold (1994) found a sex difference in GABA-like immunoreactivity in HVC and RA. Two independent studies concluded that the GABA-like cells are likely to be local interneurons (Paton et al., 1985; Pinaud and Mello, 2007). As they form local networks by making synapses with neighboring cells, interneurons increase complexity and might affect the local diffusion properties. Based on these properties and the assumption that HVC contains more interneurons in males compared to females, the interneurons might also contribute to a lower FA in male zebra finches as observed in the voxel-based analysis.

Gurney (1982) investigated the effects of early hormone treatment on sexual differentiation of the zebra finches' brain and behavior. In normally reared female zebra finches, HVC and RA neurons are smaller and less well-separated compared to the large-bodied and spaciously spread neurons reported in males (Gurney, 1982). Combining findings obtained by Nixdorf-Bergweiler (1996) and Kirn and De Voogd (1989) suggests that in HVC and RA neuronal density is larger in female compared to male birds at 60 dph. These sex differences in soma size (M > F) and cell density (M < F) were also confirmed by others (Bender and Veney, 2008; Bottjer et al., 1986; Grisham and Arnold, 1995; Konishi and Akutagawa, 1988; Nottebohm and Arnold, 1976b; Wade and Arnold, 2004). The surface/volume ratio of cells which is inherently coupled to cell size, is an important factor as the density and spatial organization of 'physical barriers' such as membranes greatly affect the overall diffusion properties of the tissue making diffusion MRI – especially MD – a highly sensitive probe to detect variation in cell size (Le Bihan, 2007). Therefore, the sex differences in cell density and soma size might be related to the observed difference in MD.

4.1.2.2. LMAN. In contrast to Area X, HVC and RA, LMAN shows anatomical contrast on the 3D RARE used for spatial normalization. Consequently, any differences in size or shape might be eliminated by the registration procedure leaving only differences in intrinsic tissue properties to be detected. This, however, does not affect the biological interpretation of the result as several independent studies have confirmed that the size of LMAN is similar between male and female birds (Nixdorf-Bergweiler and von Bohlen und Halbach, 2004; Nixdorf-Bergweiler, 1996, 2001). In addition, no sex difference in myelination have been found in LMAN (Nixdorf-Bergweiler and von Bohlen und Halbach, 2004). Interestingly, Nixdorf-Bergweiler (1996) performed detailed stereological analysis focused on LMAN and found that adult females displayed a higher neuronal density in LMAN (*i.e.* 91% more neurons per unit volume compared to male zebra finches (Nixdorf-Bergweiler, 1996)). Even though brain tissue is comprised of more than only neurons, these vast differences might contribute to the observed differences in MD.

In conclusion, even though only suggestions of the biological mechanisms underlying the observed differences can be made based on the DTI findings, the clusters detected with the voxel-based analysis clearly align with established findings. In addition, the voxel-based analysis yields detailed insight into the spatial extent of the sex differences. Therefore, we conclude that the optimized protocol is sensitive enough to detect known male-female differences in the adult zebra finch brain.

4.2. Implementation of DTI – methodological considerations

Fast sequences that are often used for DTI experiments in mammals cannot be readily adopted in songbirds because of certain

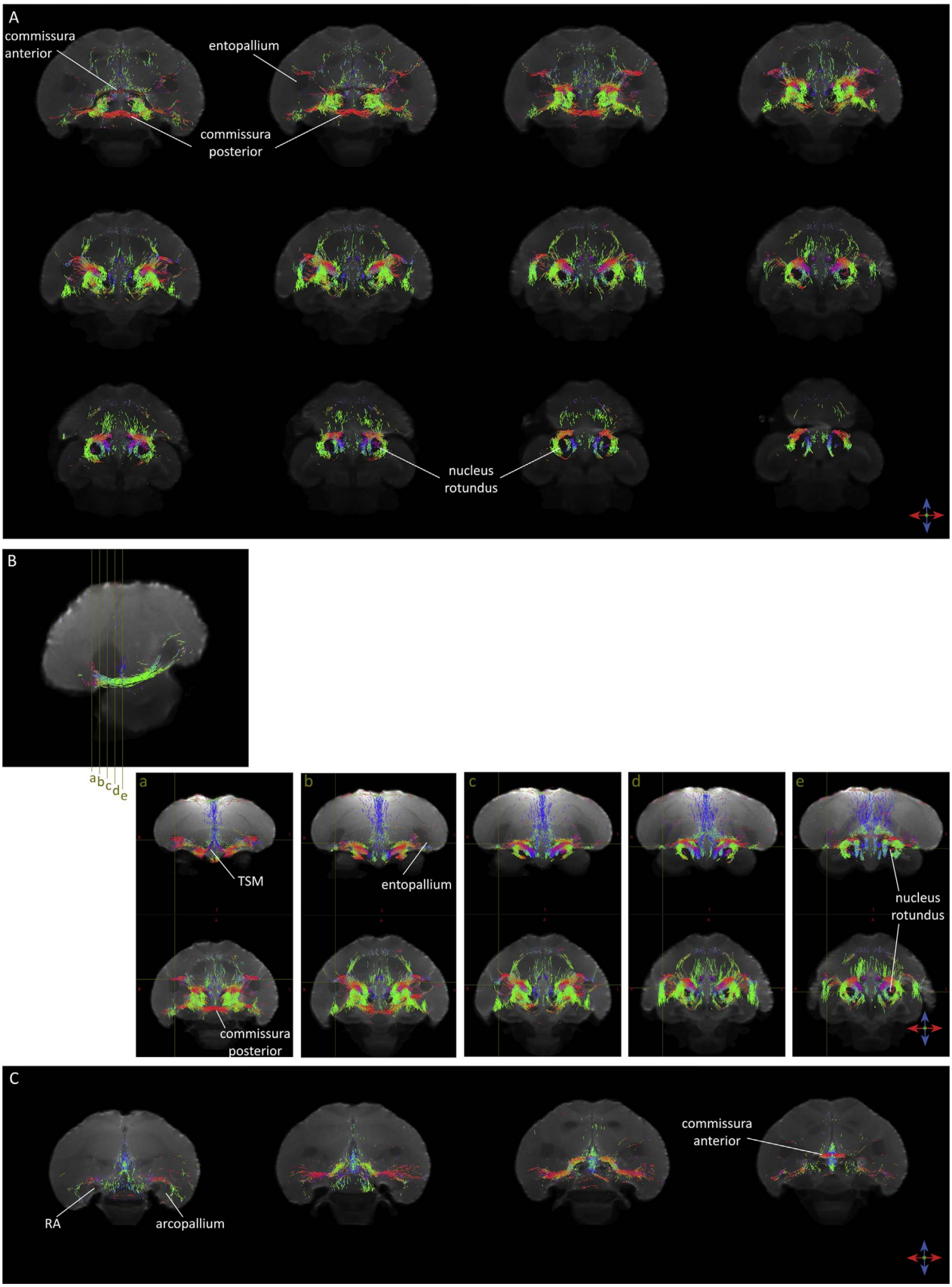

Fig. 10. Seed-based tractography in the entopallium and the commissura anterior. Tractography in (A) nucleus rotundus (seed 1 and 2), (B) nucleus rotundus (seed 1 and 2) to entopallium (seed 3 and 4), and (C) commissura anterior (seed 1 midsagittal) to arcopallium. For each anatomical region, one seed was placed in the left and a second separate seed was placed in the right hemisphere except for the the commissura anterior.

physiological properties inherent to songbird neuroanatomy ((De Groof et al., 2006); for example, the air cavities in the skull). Using a four-shot EPI sequence (Porter and Heidemann, 2009), most severe image artifacts were overcome except for brain areas near the caudal parts of the songbird brain lateral to the cerebellum. This area corresponds to the arcopallium which contains RA. As the imaging artifacts are slightly different for each bird and no opposite phase encoding polarity data were acquired (Andersson et al., 2003; Holland et al., 2010), the image distortions could not be corrected. In addition, the field maps were not used to unwarp the artifacts (Chen et al., 2006).

The 3D RARE suffers less susceptibility artifacts and yields more anatomical contrast compared to the DTI b_0. Consequently, the 3D RARE was used to improve spatial normalization to the *ex vivo* zebra finch atlas (Poirier et al., 2008). However, the difference in susceptibility artifacts led to a suboptimal alignment of the DTI and 3D RARE scans near the arcopallium. Therefore, spatial normalization might be imperfect in this region which might explain why only very weak voxel-based differences could be detected near RA.

4.3. Ex vivo SRR-DTI

The primary goal of this study was to implement an *in vivo* DTI protocol that allows to explore macro- and microstructural tissue characteristics of the zebra finch brain on a reasonable time frame. However, to further clarify observations detected *in vivo* and explore songbird neuroanatomy in greater detail, *ex vivo* DTI was opted.

Most *ex vivo* DTI protocols result in images with very high spatial resolution, however, often only 6–12 diffusion gradient directions are acquired. The most obvious reason for this are the often long acquisition times. To surpass the trade-off between acquisition time, spatial resolution and SNR inherent to DTI, we chose to employ a recently developed SRR method to acquire high-resolution DTI data (Van Steenkiste et al., 2016).

4.3.1. Bypassing the trade-off

The *ex vivo* zebra finch atlas published by Poirier et al. (2008) was acquired in 54.6 h. The *ex vivo* data sets presented here were obtained within approximately 28 or 44 h, while containing both T_2-weighted anatomical information (SRR-b_0) and DTI data which included 60 or 90 diffusion gradient directions, respectively. Visual comparison of the *ex vivo* atlas by Poirier and the SRR-b_0 images of the male bird showed that most brain areas can be identified in both data sets (Fig. 4). In addition, the overall image contrast of the SRR-b_0 images relates more closely to the 3D RARE data sets acquired *in vivo* compared to the atlas (data not shown). Furthermore, as both the *ex vivo* atlas and the SRR-b_0 of the male sample provide similar information, the SRR-b_0 image of the female brain can serve as the first MRI-based atlas of the female zebra finch brain.

If only the SRR-b_0 images had been acquired, the total acquisition time would be 6.29 or 4.67 h to obtain a T2-weighted data set with isotropic resolution of 80 μm. However, if the goal is to acquire high resolution T2-weighted data sets in a (relatively) short time span, then the number of acquisition angles (set of low resolution data sets) can be reduced even further. In this case (in plane resolution 0.078 mm, slice thickness 0.320 mm), the minimal number of low resolution data sets necessary to enable a reconstruction is 7 (based on anisotropy factor (Van Steenkiste et al., 2016)), which corresponds to approximately 2.8 hours of scanning time, without using a fast imaging sequence. This is coming very close to high-resolution *in vivo* scanning times. This could be of great interest for 'high-throughput' studies investigating subtle changes in brain volume or shape following training or along the course of pathology.

Still, depending on the goal of the study, *in vivo* imaging might not provide sufficient anatomical contrast or detail. Lerch and colleagues (2012) nicely reviewed how to choose between *in* and *ex vivo* acquisition when investigating changes in neuroanatomy (Lerch et al., 2012; Mackenzie-Graham, 2012). Therefore, the method proposed by Van Steenkiste and colleagues can markedly increase efficiency.

4.3.2. Qualitative assessment of sex differences on the ex vivo SRR-b0's

The female SRR-b_0 data set shows similar contrast compared to the male data set, however, Area X, RA and HVC cannot be localized. Concerning Area X, this is in line with previous histological studies, where Nissl stained tissue sections also appear to lack this part of the song control system in female zebra finches. HVC and RA, on the other hand, are known to be smaller in females, however, they should be discernable on the *ex vivo* data set (Nixdorf-Bergweiler, 1996). A possible explanation for this might be that HVC and RA in the female brain accumulate the gadolinium differently. The sex difference in cell density and cell spacing might lead to a differential accumulation of the contrast agent as gadoterate meglumine resides in the extracellular matrix (Marty et al., 2013; Reisinger et al., 2008). Partial volume effects are less likely to lay at the basis as several laminae and small brain areas such as the nucleus ovoidalis can be clearly found on both the male and female data sets (volume of nucleus ovoidalis appr. 0.07 mm^3 (Poirier et al., 2008) compared to 0.07–0.10 mm^3 and 0.05–0.08 mm^3 for respectively female RA and female HVC (Bottjer et al., 1985; Nixdorf-Bergweiler, 1996)).

4.3.3. Structural connectivity of the zebra finch brain

The TDI method proposed by Calamante et al. (2010) enables unraveling fiber complexity on a subvoxel level. Combined with the SRR-DTI technique, the resulting high-resolution data set (*i.e.* (40x40×40) μm^3), provides highly valuable information on the 3-dimensional organization of structural connectivity of the zebra finch brain almost up to the mesoscale level.

The TD maps illustrate that –due to its nuclear instead of laminar organization (Karten and Shimizu, 1989) – the songbird brain serves as an excellent model for DTI and tractography (De Groof and Van der Linden, 2010). The song control, auditory and visual systems consist of sets of interconnected nuclei where each component appears to be surrounded by a fiber-containing capsula. The CC TD maps provide a clear view on the song control nuclei which cannot be distinguished on T2-weighted data sets without contrast enhancement (Fig. 8; (Van der Linden et al., 1998)). Furthermore, near the optical lobes (TeO) the TD maps clearly show a fiber organization reminiscent of the orientation of myelinated fibers in the mammalian cortex (perpendicular to the cortical surface). Interestingly, the radial organization of fibers in the optical lobes is in accordance with myelin-stained histological sections (Fig. 7). Besides anatomical contrast on specific brain areas, the CC TD maps exhibit a clear view on the major subdivisions of the brain. Several laminae (*i.e.* lamina frontalis suprema and superior, lamina mesopallialis and lamina palio-subpallialis), split the songbird telencephalon in different subareas (*i.e.* hyperpallium, nidopallium, mesopallium, striatum (Fig. 8) (Karten et al., 2013; Nixdorf-Bergweiler and Bischof, 2007)).

The results of the seed-based tractography provide highly symmetrical results, and, besides Area X, most results of tractography are similar between the male and female brain. As DTI-based tractography deduces axonal geometry from the diffusion properties of water molecules in tissues, anatomical accuracy can only be validated by parallel analysis of histological tracer studies (Aurobrata and Rachid, 2016; Jbabdi and Johansen-Berg, 2011). (Azadbakht et al., 2015; Calabrese et al., 2015; Dauguet et al., 2007; Dyrby et al., 2007; Thomas et al., 2014).

Seed-based tractography of telencephalic brain areas produced streamlines that were strictly confined to the ipsilateral hemisphere. The only clear left-right connection at the level of the telencephalon detected in this study was found in the commissura anterior which could be clearly traced back to the arcopallium via the tractus OM

(Fig. 10). This 'lack' of left-right connectivity in the telencephalon has been demonstrated by neuroanatomists (Wild, 1997). When seeding tracts in more ventrally positioned brain areas such as the nucleus rotundus, an important relay center for processing of visual information, the resulting streamlines appear to travel to the contralateral hemisphere passing the commissura posterior and, to a lesser extent, the commissura anterior (Fig. 10). This observation contrasts with previous findings. Even though nucleus rotundus receives input from the TeO of both the ipsi- and contralateral hemispheres (Karten and Revzin, 1966; Schmidt and Bischof, 2001), no tracer studies report on the existence of a connection between left and right nucleus rotundus. Furthermore, the streamlines seeded in nucleus rotundus do not reach the TeO, consequently the resulting trans-hemispheric connection appears misleading. This might be attributed to parameter settings or suboptimal placement of the seed (Thomas et al., 2014). Interestingly however, the estimated fiber profile appears to end near the rostral part of the entopallium. This projection might pertain to the tectofugal pathway, where after passing nucleus rotundus fibers travel to the entopallium via the FPL (Karten and Hodos, 1970).

Besides the Area X-DLM connection no other pathways that directly connect consecutive song control system nuclei could be traced. This might partly be explained as several pathways are (assumed to be) embedded in the laminae (*e.g.* the first part of the anterior forebrain pathway (HVC to Area X projection) partly resides in the LaM (De Groof et al., 2006)). Consequently, the tracking algorithm needs to identify the appropriate subpart of the lamina that contains the fibers heading to the next relay center of the circuitry. The HVC to RA tract, on the other hand, is too diffusely and randomly organized in zebra finches to detect by DTI (Konishi and Akutagawa, 1985; Mooney and Rao, 1994; Wang et al., 1999). In addition, the songbird brain is characterized by a highly topographical organization which might also be responsible for the difficulties in finding structural tracts connecting distinct brain areas, even at this resolution.

5. Conclusion

The observed differences in LMAN and HVC are in line with previous histological investigations. Interestingly, the disparities surrounding but not including Area X and the part of the tractus OM are complementary to previous histological findings. Consequently, we conclude that the *in vivo* DTI protocol is sensitive enough to detect known sex differences in the adult zebra finch brain. This *in vivo* protocol enables future longitudinal studies where microstructural rearrangements can be traced over time within the same subject, where differences in tissue microarchitecture or connectivity might be related to the precise stage of vocal learning or upon treatment. *Ex vivo* SRR-DTI and TDI provide an unprecedented 3-dimensional overview of the overall organization of the zebra finch brain – including the female brain– with clear anatomical contrast on the song control circuitry.

Acknowledgements

We would like to thank Professor Harvey Karten for providing access to the schematic atlas drawings of the zebra finch brain. This research was supported by grants from the Research Foundation—Flanders (FWO, Project nos. G030213N, G044311N and G037813N), the Hercules Foundation (Grant no. AUHA0012), Concerted Research Actions (GOA Funding) from the University of Antwerp, Interuniversity Attraction Poles (IAP) initiated by the Belgian Science Policy Office ('PLASTOSCINE': P7/17) and an HFSP grant (HFSP-RGP0006/2015 Wildcog) to AVdL, CAC, JS and MV.

References

Andersson, J.L.R., Skare, S., Ashburner, J., 2003. How to correct susceptibility distortions in spin-echo echo-planar images: application to diffusion tensor imaging. NeuroImage 20, 870–888.

Aronov, D., Andalman, A.S., Fee, M.S., 2008. A specialized forebrain circuit for vocal babbling in the Juvenile songbird. Science 320, 630–634.

Aurobrata, G., Rachid, D., 2016. A survey of current trends in diffusion MRI for structural brain connectivity. J. Neural Eng. 13, 011001.

Azadbakht, H., Parkes, L.M., Haroon, H.A., Augath, M., Logothetis, N.K., de Crespigny, A., D'Arceuil, H.E., Parker, G.J.M., 2015. Validation of high-resolution tractography against *in vivo* tracing in the Macaque visual cortex. Cereb. Cortex..

Bai, Y., Alexander, D.C., 2008. Model-based registration to correct for motion between acquisitions in diffusion MR imaging. In: Proceedings of the Paper presented at: Biomedical Imaging: From Nano to Macro, 2008 ISBI 2008 5th IEEE International Symposium on.

Ball, G.F., Macdougall-Shackleton, S.A., 2001. Sex differences in songbirds 25 years later: what have we learned and where do we go? Microsc. Res. Technol. 54, 327–334.

Bender, A.T., Veney, S.L., 2008. Treatment with the specific estrogen receptor antagonist ICI 182,780 demasculinizes neuron soma size in the developing zebra finch brain. Brain Res. 1246, 47–53.

Bottjer, S., Miesner, E., Arnold, A., 1984. Forebrain lesions disrupt development but not maintenance of song in passerine birds. Science 224, 901–903.

Bottjer, S., Glaessner, S., Arnold, A., 1985. Ontogeny of brain nuclei controlling song learning and behavior in zebra finches. J. Neurosci. 5, 1556–1562.

Bottjer, S.W., Miesner, E.A., Arnold, A.P., 1986. Changes in neuronal number, density and size account for increases in volume of song-control nuclei during song development in zebra finches. Neurosci. Lett. 67, 263–268.

Brainard, M.S., Doupe, A.J., 2000. Interruption of a basal ganglia-forebrain circuit prevents plasticity of learned vocalizations. Nature 404, 762–766.

Brainard, M.S., Doupe, A.J., 2013. Translating birdsong: songbirds as a model for basic and applied medical research. Annu. Rev. Neurosci. 36, 489–517.

Calabrese, E., Badea, A., Cofer, G., Qi, Y., Johnson, G.A., 2015. A diffusion MRI tractography connectome of the mouse brain and comparison with neuronal tracer data. Cereb. Cortex.

Calamante, F., Tournier, J.-D., Jackson, G.D., Connelly, A., 2010. Track-density imaging (TDI): super-resolution white matter imaging using whole-brain track-density mapping. NeuroImage 53, 1233–1243.

Caruyer, E., Lenglet, C., Sapiro, G., Deriche, R., 2013. Design of multishell sampling schemes with uniform coverage in diffusion MRI. Magn. Reson. Med. 69, 1534–1540.

Chen, B., Guo, H., Song, A.W., 2006. Correction for direction-dependent distortions in diffusion tensor imaging using matched magnetic field maps. NeuroImage 30, 121–129.

Cornez, G., ter Haar, S.M., Cornil, C.A., Balthazart, J., 2015. Anatomically discrete sex differences in neuroplasticity in zebra finches as reflected by perineuronal nets. PLoS One 10, e0123199.

Dauguet, J., Peled, S., Berezovskii, V., Delzescaux, T., Warfield, S.K., Born, R., Westin, C.-F., 2007. Comparison of fiber tracts derived from *in-vivo* DTI tractography with 3D histological neural tract tracer reconstruction on a macaque brain. NeuroImage 37, 530–538.

De Groof, G., Van der Linden, A., 2010. Love songs, bird brains and diffusion tensor imaging. NMR Biomed. 23, 873–883.

De Groof, G., Verhoye, M., Van Meir, V., Balthazart, J., Van der Linden, A., 2008. Seasonal rewiring of the songbird brain: an in vivo MRI study. Eur. J. Neurosci. 28, 2475–2485.

De Groof, G., Verhoye, M., Van Meir, V., Tindemans, I., Leemans, A., Van der Linden, A., 2006. *In vivo* diffusion tensor imaging (DTI) of brain subdivisions and vocal pathways in songbirds. NeuroImage 29, 754–763.

De Groof, G., Verhoye, M., Poirier, C., Leemans, A., Eens, M., Darras, V.M., Van der Linden, A., 2009. Structural changes between seasons in the songbird auditory forebrain. J. Neurosci. 29, 13557–13565.

Doupe, A.J., Kuhl, P.K., 1999. BIRDSONG AND HUMAN SPEECH: common themes and mechanisms. Annu. Rev. Neurosci. 22, 567–631.

Dyrby, T.B., Søgaard, L.V., Parker, G.J., Alexander, D.C., Lind, N.M., Baaré, W.F.C., Hay-Schmidt, A., Eriksen, N., Pakkenberg, B., Paulson, O.B., et al., 2007. Validation of in vitro probabilistic tractography. NeuroImage *37*, 1267–1277.

Grisham, W., Arnold, A.P., 1994. Distribution of GABA-like immunoreactivity in the song system of the zebra finch. Brain Res. 651, 115–122.

Grisham, W., Arnold, A.P., 1995. A direct comparison of the masculinizing effects of testosterone, androstenedione, estrogen, and progesterone on the development of the zebra finch song system. J. Neurobiol. 26, 163–170.

Gurney, M., 1981. Hormonal control of cell form and number in the zebra finch song system. J. Neurosci. 1, 658–673.

Gurney, M.E., 1982. Behavioral correlates of sexual differentiation in the zebra finch song system. Brain Res. 231, 153–172.

Holland, D., Kuperman, J.M., Dale, A.M., 2010. Efficient correction of inhomogeneous static magnetic field-induced distortion in echo planar imaging. NeuroImage 50, 175 .

Jarvis, E.D., 2004. Learned birdsong and the neurobiology of human language. Ann. N. Y. Acad. Sci. 1016, 749–777.

Jarvis, E.D., Gunturkun, O., Bruce, L., Csillag, A., Karten, H., Kuenzel, W., Medina, L., Paxinos, G., Perkel, D.J., Shimizu, T., et al., 2005. Avian brains and a new understanding of vertebrate brain evolution. Nat. Rev. Neurosci. 6, 151–159.

Jbabdi, S., Johansen-Berg, H., 2011. Tractography – where do we go from here? Brain Connect. 1, 169–183.

Jeurissen, B., Tournier, J.-D., Dhollander, T., Connelly, A., Sijbers, J., 2014. Multi-tissue constrained spherical deconvolution for improved analysis of multi-shell diffusion MRI data. NeuroImage 103, 411–426.

Jones, D.K., Horsfield, M.A., Simmons, A., 1999. Optimal strategies for measuring diffusion in anisotropic systems by magnetic resonance imaging. Magn. Reson. Med. 42, 515–525.
Karten, H.J., Revzin, A.M., 1966. The afferent connections of the nucleus rotundus in the pigeon. Brain Res. 2, 368–377.
Karten, H.J., Hodos, W., 1970. Telencephalic projections of the nucleus rotundus in the pigeon (Columba livia). J. Comput. Neurol. 140, 35–51.
Karten, H.J., Shimizu, T., 1989. The origins of neocortex: connections and lamination as distinct events in evolution. J. Cogn. Neurosci. 1, 291–301.
Karten, H.J., Brzozowska-Prechtl, A., Lovell, P.V., Tang, D.D., Mello, C.V., Wang, H., Mitra, P.P., 2013. Digital atlas of the zebra finch (Taeniopygia guttata) brain: a high resolution photo atlas. J. Compar. Neurol. 521, 3702–3715.
Kirn, J., DeVoogd, T., 1989. Genesis and death of vocal control neurons during sexual differentiation in the zebra finch. J. Neurosci. 9, 3176–3187.
Konishi, M., Akutagawa, E., 1985. Neuronal growth, atrophy and death in a sexually dimorphic song nucleus in the zebra finch brain. Nature 315, 145–147.
Konishi, M., Akutagawa, E., 1988. A critical period for estrogen action on neurons of the song control system in the zebra finch. Proc. Natl. Acad. Sci. USA 85, 7006–7007.
Le Bihan, D., 2007. The 'wet mind': water and functional neuroimaging. Phys. Med. Biol. 52, R57.
Lerch, J.P., Gazdzinski, L., Germann, J., Sled, J.G., Henkelman, R.M., Nieman, B.J., 2012. Wanted dead or alive? The tradeoff between *in-vivo versus ex-vivo* MR brain imaging in the mouse. Front. Neuroinform., 6.
MacDougall-Shackleton, S.A., Ball, G.F., 1999. Comparative studies of sex differences in the song-control system of songbirds. Trends Neurosci. 22, 432–436.
Mackenzie-Graham, A., 2012. *In Vivo versus Ex Vivo* magnetic resonance imaging in mice. Front. Neuroinform., 6.
Marty, B., Djemaï, B., Robic, C., Port, M., Robert, P., Valette, J., Boumezbeur, F., Le Bihan, D., Lethimonnier, F., Mériaux, S., 2013. Hindered diffusion of MRI contrast agents in rat brain extracellular micro-environment assessed by acquisition of dynamic T1 and T2 maps. Contrast Media Mol. Imaging 8, 12–19.
Meyer, C.E., Boroda, E., Nick, T.A., 2014. Sexually dimorphic perineuronal net expression in the songbird. Basal Ganglia 3, 229–237.
Mooney, R., Rao, M., 1994. Waiting periods *versus* early innervation: the development of axonal connections in the zebra finch song system. J. Neurosci. 14, 6532–6543.
Mori, S., Zhang, J., 2006. Principles of diffusion tensor imaging and its applications to basic neuroscience research. Neuron 51, 527–539.
Nixdorf-Bergweiler, B., von Bohlen und Halbach, V., 2004. Major sex differences in the development of myelination are prominent in song system nucleus HVC but not lMAN. Anim. Biol. 54, 27–43.
Nixdorf-Bergweiler, B.E., 1996. Divergent and parallel development in volume sizes of telencephalic song nuclei in and female zebra finches. J. Comput. Neurol. 375, 445–456.
Nixdorf-Bergweiler, B.E., 2001. Lateral magnocellular nucleus of the anterior neostriatum (LMAN) in the zebra finch: neuronal connectivity and the emergence of sex differences in cell morphology. Microsc. Res. Technol. 54, 335–353.
Nixdorf-Bergweiler, B., Bischof, H.-J., 2007. Atlas of The Brain of The Zebra Finch, Taeniopygia Guttata: With Special Emphasis on Telencephalic Visual and Song System Nuclei in Transverse and Sagittal Sections.
Nottebohm, F., Arnold, A., 1976a. Sexual dimorphism in vocal control areas of the songbird brain. Science 194, 211–213.
Nottebohm, F., Arnold, A.P., 1976b. Sexual dimorphism in vocal control areas of the songbird brain. Science 194, 211–213.
Ölveczky, B.P., Andalman, A.S., Fee, M.S., 2005. Vocal experimentation in the Juvenile songbird requires a Basal Ganglia circuit. PLoS Biol. 3, e153.
Paton, J., O'Loughlin, B., Nottebohm, F., 1985. Cells born in adult canary forebrain are local interneurons. J. Neurosci. 5, 3088–3093.
Person, A.L., Gale, S.D., Farries, M.A., Perkel, D.J., 2008. Organization of the songbird basal ganglia, including area X. J. Comput. Neurol. 508, 840–866.
Pinaud, R., Mello, C.V., 2007. GABA immunoreactivity in auditory and song control brain areas of zebra finches. J. Chem. Neuroanat. 34 (1), 1–2.
Poirier, C., Vellema, M., Verhoye, M., Van Meir, V., Wild, J.M., Balthazart, J., Van Der Linden, A., 2008. A three-dimensional MRI atlas of the zebra finch brain in stereotaxic coordinates. NeuroImage 41, 1–6.
Poot, D.H.J., Van Meir, V., Sijbers, J., 2010. General and efficient super-resolution method for multi-slice MRI. In: Jiang, T., Navab, N., Pluim, J.W., Viergever, M. (Eds.), Medical Image Computing and Computer-Assisted Intervention – MICCAI 2010. Springer, Berlin Heidelberg, 615–622.
Porter, D.A., Heidemann, R.M., 2009. High resolution diffusion-weighted imaging using readout-segmented echo-planar imaging, parallel imaging and a two-dimensional navigator-based reacquisition. Magn. Reson. Med. 62, 468–475.
Reiner, A., Laverghetta, A.V., Meade, C.A., Cuthbertson, S.L., Bottjer, S.W., 2004. An immunohistochemical and pathway tracing study of the striatopallidal organization of area X in the male zebra finch. J. Comput. Neurol. 469, 239–261.
Reisinger, C., Gluecker, T., Jacob, A.L., Bongartz, G., Bilecen, D., 2008. Dynamic magnetic resonance angiography of the arteries of the hand. A comparison between an extracellular and an intravascular contrast agent. Eur. Radiol. 19, 495–502.
Scharff, C., Nottebohm, F., 1991. A comparative study of the behavioral deficits following lesions of various parts of the zebra finch song system: implications for vocal learning. J. Neurosci. 11, 2896–2913.
Schmidt, A., Bischof, H.-J., 2001. Integration of information from both eyes by single neurons of nucleus rotundus, ectostriatum and lateral neostriatum in the zebra finch (Taeniopygia guttata castanotis Gould). Brain Res. 923, 20–31.
Simpson, H., Vicario, D., 1990. Brain pathways for learned and unlearned vocalizations differ in zebra finches. J. Neurosci. 10, 1541–1556.
Tax, C.M.W., Jeurissen, B., Vos, S.B., Viergever, M.A., Leemans, A., 2014. Recursive calibration of the fiber response function for spherical deconvolution of diffusion MRI data. NeuroImage 86, 67–80.
Thomas, C., Ye, F.Q., Irfanoglu, M.O., Modi, P., Saleem, K.S., Leopold, D.A., Pierpaoli, C., 2014. Anatomical accuracy of brain connections derived from diffusion MRI tractography is inherently limited. Proc. Natl. Acad. Sci. USA 111, 16574–16579.
Toga, A.W., Thompson, P.M., 2003. Mapping brain asymmetry. Nat. Rev. Neurosci. 4, 37–48.
Tournier, J.D., Calamante, F., Connelly, A., 2007. Robust determination of the fibre orientation distribution in diffusion MRI: non-negativity constrained super-resolved spherical deconvolution. NeuroImage 35, 1459–1472.
Tournier, J.D., Calamante, F., Connelly, A., 2012. MRtrix: diffusion tractography in crossing fiber regions. Int. J. Imaging Syst. Technol. 22, 53–66.
Tournier, J.C., F., Connelly, A., 2010. Improved probabilistic streamlines tractography by 2nd order integration over fibre orientation distributions. Paper presented at: International Society for Magnetic Resonance in Medicine (ISMRM), Stockholm.
Van der Linden, A., Verhoye, M., Van Audekerke, J., Peeters, R., Eens, M., Newman, S.W., Smulders, T., Balthazart, J., DeVoogd, T.J., 1998. Noninvasive in vivo anatomical studies of the oscine brain by high resolution MRI microscopy. J. Neurosci. Methods 81, 45–52.
Van Steenkiste, G., Jeurissen, B., Veraart, J., den Dekker, A.J., Parizel, P.M., Poot, D.H.J., Sijbers, J., 2016. Super-resolution reconstruction of diffusion parameters from diffusion-weighted images with different slice orientations. Magn. Reson. Med. 75, 181–195.
Verhoye, M., Van der Linden, A., Van Audekerke, J., Sijbers, J., Eens, M., Balthazart, J., 1998. Imaging birds in a bird cage: *in-vivo* FSE 3D MRI of bird brain. Magn. Reson. Mater. Phys. Biol. Med. 6, 22–27.
Wade, J., Arnold, A.P., 2004. Sexual differentiation of the zebra finch song system. Ann. N. Y. Acad. Sci. 1016, 540–559.
Wang, J., Sakaguchi, H., Sokabe, M., 1999. Sex differences in the vocal motor pathway of the zebra finch revealed by real-time optical imaging technique. NeuroReport 10, 2487–2491.
Wild, J.M., 1993. Descending projections of the songbird nucleus robustus archistriatalis. J. Comput. Neurol. 338, 225–241.
Wild, J.M., 1997. Neural pathways for the control of birdsong production. J. Neurobiol. 33, 653–670.
Yu, A.C., Margoliash, D., 1996. Temporal hierarchical control of singing in birds. Science 273, 1871–1875.
Zatorre, R.J., Fields, R.D., Johansen-Berg, H., 2012. Plasticity in gray and white: neuroimaging changes in brain structure during learning. Nat. Neurosci. 15, 528–536.